Ocean Dynamics (2023) 73:517–529
https://doi.org/10.1007/s10236-023-01563-x

Analysis of the dynamic mechanisms of upwelling in deep ocean water caused by typhoons

Famei Lei[1] · **Hao Dai**[1] · **Shaoping Shang**[1] · **Zhigang He**[1] · **Shuai Yang**[1]

Received: 18 April 2022 / Accepted: 20 June 2023 / Published online: 13 July 2023

Abstract
A typhoon (hurricane) is a very strong local disturbance that can affect ocean water as deep as 1000 m. According to observations and numerical simulations, the decrease in ocean temperature is believed to be caused by inertial pumping, entrainment, upwelling, and a pressure-gradient force; however, these assumptions are mostly based on modeling and do not have a clear dynamic mechanism. Therefore, in this study, the dynamic mechanism of ocean water in a highly-idealized ocean and wind field was calculated. Within the maximum wind range, downwelling in the ocean surface is caused as per the classical Ekman layer transport. Then, a pressure-gradient force drives a cyclo-geostrophic current. Because it provides centripetal force, the pressure-gradient force decreases with increasing depth. These different currents generate friction that is similar to bottom Ekman pumping, leading to upwelling. In the actual ocean, the pressure-gradient force is not only balanced by centripetal force but also baroclinic force. When these forces are balanced, the pressure-gradient force disappears, and the dynamic motion of the ocean water stops. Thus, upwelling no longer occurs. The depth at which this balance occurs is considered to be the maximum depth that a typhoon can impact. Therefore, the pressure-gradient force, caused by typhoons and then offset by centripetal and baroclinic forces, is the original dynamic of upwelling in deep ocean water.

Keywords Upwelling · Typhoon · Ekman layer · Pressure gradient force · Centripetal force

1 Introduction

A typhoon is a very strong local disturbance that injects momentum into the ocean and removes heat via movement, causing significant abnormal changes in dynamics and thermotics over a very short duration (Zheng et al. 2006). Therefore, typhoons significantly impact the heat exchange, mixing, and ecological processes in the upper ocean, including massive waves, increased heat transport (Emanuel 2003; Jansen and Ferrari 2009), deepening of the mixed layer (Liu et al. 2007), increased chlorophyll concentration (Lin et al. 2003), intense vertical mixing (Wada et al. 2009), strong wind-driven currents (Price 1981, 1983), and storm surges.

The response of the upper ocean layer to typhoons is a classic issue for the physical oceanography community, and numerous studies have been conducted on it. In 1964, Hurricane Hilda in the Gulf of Mexico was comprehensively observed (Leipper 1967). Leipper found that the suction of the typhoon center could reach 60 m deep, transporting the surface seawater outward before it sank at the typhoon edge. A fixed-point buoy deployed by Taitra et al. (1993) recorded a typhoon process at close range, providing a rare vertical-temperature distribution. It was found that the temperature at the surface cooled continuously during a typhoon but rose at 50 m and 100 m depths. Then, after warming up slightly, it returned to the original temperature.

Satellite observations suggest that hurricane-induced phytoplankton blooms may be the result of nutrient upwelling from significant depths as 100 m (Babin et al. 2004; Gierach and Subrahmanyam 2008). Brooks (1983) concluded that the vertical scale of ocean response in the Gulf of Mexico after Hurricane Allen in 1980 was much larger than the depth of the 200 m thermocline. Pudov (1978) showed that ocean water from a depth of 240 m upwelled near the track of Typhoon Tess (1975). Hurricane Frederic induced ocean

✉ Famei Lei
lfm101659@163.com

✉ Shaoping Shang
spshang@xmu.edu.com

[1] Institute of Ocean Exploration Technology, College of Ocean and Earth Sciences, Xiamen University, Xiamen, China

currents at least as deep as 450 m (Hopkins 1982). Moreover, in some special cases, typhoons have even impacted significant depths as 1000 m (Spencer et al. 2016).

Ocean upwelling mechanism has been extensively researched both theoretically and practically, producing some significant results. A few observations have shown that the deep ocean response to a moving hurricane exists in the form of near-inertial oscillation (Shay and Elsberry 1987; Morozov and Velarde 2008). Price et al. (1994) indicated that upwelling is driven by the wind stress curl of the hurricane through divergent transport in the upper-ocean, with inertial pumping causing the divergence and associated upwelling and downwelling in the mixed-layer (Price 1983). Wada (2005) concluded that a rapid decrease in sea-surface temperature is caused by enhanced entrainment, whereas sea-surface cooling under slow transport is induced not only by entrainment but also by upwelling. Based on an oceanic analysis, Babin et al. (2004) found that the chlorophyll-a enhancement induced by a hurricane was associated with the upwelling of cold water from the deep ocean. Lu and Huang (2010) studied a stationary hurricane in a homogenous ocean and found that ocean flow converges in an inward spiral in the deeper layer, while it diverges in the upper layer. Zhang et al. (2016) used a three-dimensional numerical model to compare the in-situ observations of typhoon Kalmaegi (2014) to show that the dynamic response of the ocean is characterized by strong near-inertial currents with opposite phases in the surface mixed layer and thermocline. In addition, they observed a dominant excitation response in the first baroclinic mode of the thermocline.

However, there are few studies observing typhoons, and current observation data are mostly based on drifting or anchor buoys. Because of the limited typhoon observation data, numerical simulations are very important medium for typhoon research. Using numerical simulation, researchers have identified some mechanisms of ocean upwelling. For example, Chang (1985) pointed out that since vertical mixing cannot penetrate to such a depth in a matter of a few hours, the dynamic response in the deep ocean must be transmitted by barotropic pressure force. By employing a scale analysis of the depth-integrated momentum and continuity equations, it was found that depth-averaged currents are nearly non-divergent and are determined entirely by the wind stress (Ginis and Sutyrin 1995). Further, the upwelling beneath the center of a hurricane is supplied with mass from the radial inflow in the boundary layer by the cyclo-geostrophic current under the balance between bottom friction and the Coriolis force (Lu and Huang 2010).

Hence, there are different conclusions among them so it is of great interest to explore the impact of the hurricane on the circulation through the whole water column. Thus, in this study, we evaluated a stationary typhoon that induced a steady circulation in a homogenous environment to explain the dynamic mechanism of ocean upwelling from the deep ocean. We want to determine how the role of the typhoon reaches the deep ocean, even to the reference surface, and how it drives the deep water rising. This study is organized as follows: Sect. 2 discusses the surface Ekman layer in the highly idealized ocean, examines the role of centripetal force in the deep ocean, and estimates the depth impacted by a typhoon in the real ocean; Sect. 3 outlines the results of upwelling, and finally, Sect. 4 summarizes the conclusions.

2 Methods

2.1 Surface Ekman layer in a highly idealized ocean

2.1.1 Vertical velocity (w_s) in surface Ekman layer

First, consider the circulation in a homogenous ocean induced by a stationary typhoon. When a typhoon causes a horizontal frictional stress, an Ekman layer is formed. The wind-driven horizontal transport and velocity in the surface Ekman layer has the following components (Benoit and Beckers 2009):

$$M_{\mathrm{x}} = \int_{-d_T}^{0} \rho_0 (u - \overline{u}) dz = \frac{1}{f} \tau_{\mathrm{y}}, \tag{1.1}$$

$$M_{\mathrm{y}} = \int_{-d_T}^{0} \rho_0 (v - \overline{v}) dz = \frac{-1}{f} \tau_x, \tag{1.2}$$

$$u = \overline{u} + \frac{\sqrt{2}}{\rho_0 f d_T} e^{\frac{z}{d_T}} \left[\tau_x sin\left(\frac{\pi}{4} + \frac{z}{d_T}\right) + \tau_y cos\left(\frac{\pi}{4} + \frac{z}{d_T}\right) \right], \tag{2.1}$$

$$v = \overline{v} + \frac{\sqrt{2}}{\rho_0 f d_T} e^{\frac{z}{d_T}} \left[-\tau_x cos\left(\frac{\pi}{4} + \frac{z}{d_T}\right) + \tau_y sin\left(\frac{\pi}{4} + \frac{z}{d_T}\right) \right], \tag{2.2}$$

where M_{x} and M_y are the eastern and northern Ekman transport components, respectively; τ_{x} and τ_y are the eastern and northern wind stress values, respectively; u and v are the eastern and northern velocities, respectively; $\overline{u}$ and $\overline{v}$ are the eastern and northern interior velocities, respectively; f is the Coriolis parameter; d_T is the depth of the surface Ekman layer; and ρ_0 is the density of the ocean water.

A typhoon wind field is very complex, and it is one of the most powerful drivers of oceanic circulation. However, in this study, we assume that the typhoon wind field is axisymmetric and there is no pressure gradient in the azimuthal direction. Therefore, we can only consider the

radial direction transport by azimuthal wind stress, thereby, neglecting other influences. According to Eqs. (1.1) and (1.2), transport keeps pace with wind stress. Because wind speed increases continually from the center to the radius reaching a maximum and then decays rapidly with radius (Emanuel 2003), strong wind stress drives radial outward Ekman transport in the upper ocean, causing the ocean water to decrease inward along the radius of the maximum winds and elevate outward. For the entire typhoon, ocean water elevation fields exist with a low center and high surrounding, showed in Fig. 1.

Therefore, the circulation in the upper layer can be separated into two components: a radial outward Ekman transport driven by the typhoon, and a geostrophic current driven by the ocean water elevation field. On this basis, we can calculate the variation of vertical velocity using the continuity equation and the solution of the surface Ekman layer Eq. 2.1 Eq. 2.2. Thus, the results (the process is provided in the Appendix Eq. 36) are as follows:

$$\frac{\partial w_s}{\partial z} = -\left(\frac{\partial u}{\partial x} + \frac{\partial v}{\partial y}\right) = -\frac{\sqrt{2}}{\rho_0 f d_T} e^{\frac{z}{d_T}} \left(\frac{\partial \tau}{\partial r} + \frac{\tau}{r}\right) cos\left(\frac{\pi}{4} + \frac{z}{d_T}\right), \tag{3}$$

where w_s is the vertical velocity in the surface Ekman layer, τ is the magnitude of the wind stress, and r is the radius of circular motion. Then, the solution (the process is provided in the Appendix Eq. 38) with the boundary $w_s(z = -\infty) = 0$ is as follows:

$$w_s = -\frac{1}{\rho_0 f} e^{\frac{z}{d_T}} \left(\frac{\partial \tau}{\partial r} + \frac{\tau}{r}\right) cos\frac{z}{d_T}. \tag{4}$$

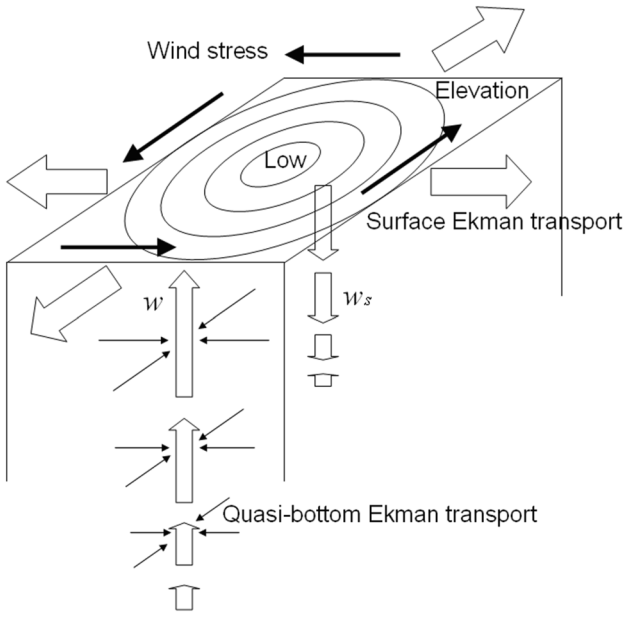

Fig. 1 Sketch of the elevation and vertical velocity caused by typhoon

It indicates that, in the northern hemisphere, from $z = 0$ to $z = -\pi d_T/2$, a counterclockwise (typhoon) generates a downwelling (w_s<0 and the curl $\partial w_s/\partial z$<0), between $z = -\pi d_T/2$ and $z = -3\pi d_T/4$, it causes a upwelling and the water also diverges, and below $z = -3\pi d_T/4$, it causes a upwelling and the water converges, showed in Fig. 1. However, the w_s decays exponentially in the vertical direction (ignored below $z = -\pi d_T$), so downwelling is much larger than upwelling and ocean water elevation in the center of typhoon will decline.

2.1.2 Ekman transport caused by pressure-gradient force

Because of the Ekman transport in the surface layer, the water elevation in the typhoon center becomes lower while that surrounding it becomes higher. The pressure-gradient force is proportional to the water elevation, driving the geostrophic current. If we only consider the balance between the Coriolis force and the pressure gradient force, we obtain the following equation:

$$fv = \frac{1}{\rho_0}\frac{\partial p}{\partial x}, \tag{5.1}$$

$$fu = -\frac{1}{\rho_0}\frac{\partial p}{\partial y}, \tag{5.2}$$

We can also calculate the variation of w_p by the following equation:

$$\frac{\partial w_p}{\partial z} = -\left(\frac{\partial u}{\partial x} + \frac{\partial v}{\partial y}\right) = 0. \tag{6}$$

where w_p is the vertical velocity caused by pressure gradient force and p is the pressure.

This shows that w_p is a constant, which indicates a non-divergence field, revealing that the geostrophic flow cannot drive upwelling or downwelling. The geostrophic current will flow with a constant velocity in a quasi-circular shape, called a cyclo-geostrophic current. Under normal conditions, the pressure-gradient force affects the entire water column from the surface to the bottom (Lu and Huang 2010). Therefore, in a homogenous ocean, a cyclo-geostrophic current will occur through the entire column regardless of water depth. Therefore, a pure geostrophic current caused by pressure-gradient force will not cause transport.

However, in reality, a typhoon cannot impact a depth exceeding the reference surface regardless of the in-situ observation or numerical model. Lu and Huang (2010) predicted that there are azimuthal cyclo-geostrophic currents between the top and bottom boundary layers, but this concept is highly idealized and has no evidence.

2.2 Role of pressure gradient force in deep ocean

To construct our framework, we started from the basic foundation. For a moving typhoon, the analytical solution for the oceanic response is highly complex, and there is currently no analytical solution. For simplicity, the vertical water column can be decomposed into two parts: Ekman transport and cyclo-geostrophic current. We assume that there is only a cyclo-geostrophic current below the Ekman depth in a homogenous ocean induced by a typhoon. As previously determined, the pure geostrophic current cannot affect the vertical velocity, but there exists some underlying cause more than the balance between the Coriolis force and pressure gradient force. Specifically, we must consider the centripetal force maintaining the circular motion of the ocean water. The dimensional analysis of pressure gradient force and centripetal force are as follows:

In the surface, the dimension of v is 1 m/s, g is 10 m/s^2, ρ is 10^3 kg/m^3, H (water elevation) is 1 m, R (the radius of maximum wind) is 10^5 m, z is 10^3 m and A_z (strong wind) is 0.1 m^2/s. Then, the dimension of pressure gradient force is $\frac{1}{\rho}\frac{\partial p}{\partial r} \sim \frac{1}{\rho}\frac{\rho g H}{R} \sim 10^{-4}$, the dimension of centripetal force is $m\frac{v^2}{r} \sim \frac{vv}{R} \sim 10^{-5}$, and the dimension of friction force is $A_z\frac{\partial^2 v}{\partial z^2} \sim A_z\frac{v}{z^2} \sim 10^{-7}$. However, in deep ocean, the dimension of v and H would be 0.1 m/s and 0.1 m. Then, the dimension of pressure gradient force is $\frac{1}{\rho}\frac{\partial p}{\partial r} \sim \frac{1}{\rho}\frac{\rho g H}{R} \sim 10^{-5}$, the dimension of centripetal force is $m\frac{v^2}{r} \sim \frac{vv}{R} \sim 10^{-7}$, and the dimension of friction force is $A_z\frac{\partial^2 v}{\partial z^2} \sim A_z\frac{v}{z^2} \sim 10^{-8}$. Therefore, the centripetal force should not be negligible, and it plays an important role, especially in the surface.

The origin of centripetal force is derived from the pressure-gradient force. Neglecting the other current and only considering the cyclo-geostrophic current, we can obtain the horizontal momentum equations in the surface layer:

$$-fv_{\theta 0} = -\frac{1}{\rho_0}\frac{\partial p_0}{\partial r}, \tag{7.1}$$

$$fv_{r0} = 0. \tag{7.2}$$

Therefore, the balance of force in the radial direction is presented as follows:

$$\frac{1}{\rho_0}\frac{\partial p}{\partial r} = \frac{1}{\rho_0}\frac{\partial p_0}{\partial r} + \frac{v_\theta^2}{r_0}, \tag{8}$$

where v_{r0} and $v_{\theta 0}$ are the radial and azimuthal velocities in the surface layer, respectively; p_0 is the rest of the p subtracted centripetal force; and r_0 is the radius of maximum circular motion. Thus, the geostrophic current can be calculated using the following equation:

$$\frac{1}{\rho_0}\frac{\partial p}{\partial r} = fv_{\theta 0} + \frac{v_{\theta 0}^2}{r_0}, \tag{9}$$

for which the solution (the other root rejected) is as follows:

$$v_{\theta 0} = \frac{-fr_0 + \sqrt{(fr_0)^2 + \frac{4r_0}{\rho_0}\frac{\partial p}{\partial r}}}{2}. \tag{10}$$

According to the surface current $v_{\theta 0}$, we can obtain the centripetal force, allowing the geostrophic current $v_{\theta 1}$ in the deeper layer to be calculated according to p_0. Then, $v_{\theta 2}$ can be calculated using p_1, $v_{\theta 3}$ by p_2, and so on. Therefore, the surface layer pressure-gradient force is caused by p, the first deeper layer is caused by p_0, and the second by p_1, until $p_n = 0$. Thus, in the entire water column, $v_{\theta i}$ can be calculated as follows:

$$v_{\theta i} = \frac{-fr_0 + \sqrt{(fr_0)^2 + \frac{4r_0}{\rho_0}\frac{\partial p_{i-1}}{\partial r}}}{2} i = 1, 2, 3, \cdots, n. \tag{11}$$

where n is the number of water column layers from surface to bottom, v_{ri} and $v_{\theta i}$ are the radial and azimuthal velocities in the i layer, respectively.

Therefore, different pressure gradient forces drive different currents. In this state, the ocean water is not only operated by the Coriolis and pressure gradient forces but also by friction. Thus, the deeper layer ocean water horizontal momentum equations change as follows:

$$-f(v - \overline{v}) = \frac{\partial}{\partial z}\left(A_z\frac{\partial u}{\partial z}\right), \tag{12.1}$$

$$f(u - \overline{u}) = \frac{\partial}{\partial z}\left(A_z\frac{\partial v}{\partial z}\right), \tag{12.2}$$

where $\overline{u}$ and $\overline{v}$ are the currents in the upper layer, and A_z is the vertical eddy viscosity.

Note that these equations are similar to the bottom Ekman layer equations and are called the quasi-bottom Ekman layer. Their solutions that satisfy the boundary conditions ($u = \overline{u}$ and $v = \overline{v}$ in the upper layer; $u = v = 0$ at the bottom) are presented as follows (Benoit and Beckers 2009):

$$u = \overline{u}\left(1 - e^{\frac{-z}{d_B}}cos\frac{z}{d_B}\right) - \overline{v}e^{\frac{-z}{d_B}}sin\frac{z}{d_B}, \tag{13.1}$$

$$v = \overline{u}e^{\frac{-z}{d_B}}sin\frac{z}{d_B} + \overline{v}\left(1 - e^{\frac{-z}{d_B}}cos\frac{z}{d_B}\right), \tag{13.2}$$

where d_B is the depth of quasi-bottom Ekman layer.

The variation of vertical velocity can be calculated as follows (the process is provided in the Appendix Eq. 37):

$$\frac{\partial w_b}{\partial z} = -\left(\frac{\partial u}{\partial x} + \frac{\partial v}{\partial y}\right) = e^{-\frac{z}{d_B}}\left(\frac{\partial v_\theta}{\partial r} + \frac{v_\theta}{r}\right) sin\frac{z}{d_B}, \tag{14}$$

where w_b is the vertical velocity in the quasi-bottom Ekman layer.

Then, the solution (the process is provided in the Appendix Eq. 38) with the boundary $w_b(z = 0)$=0 can be calculated as follows:

$$w_b = \left(\frac{\partial v_\theta}{\partial r} + \frac{v_\theta}{r}\right)\left(\frac{d_B}{2} - \frac{\sqrt{2}d_B}{2}e^{-\frac{z}{d_B}} sin\left(\frac{z}{d_B} + \frac{\pi}{4}\right)\right). \tag{15}$$

It can be seen that when $0 < z < \pi d_B$, $\partial w_b/\partial z > 0$ and $w_b > 0$. This indicates that the ocean water converges to rising and w_b increases from $z = 0$ to $z = \pi d_B$. Note that $z = 0$ is not the actual ocean bottom but the depth of p_i below πd_B.

The transport attributed to the quasi-bottom layer flow in the i layer has components given by

$$U_i = \int_0^\infty (u - \overline{u})dz = -\frac{d_B}{2}(\overline{u} + \overline{v}) \tag{16.1}$$

$$V_i = \int_0^\infty (v - \overline{v})dz = -\frac{d_B}{2}(\overline{u} - \overline{v}) \tag{16.1}$$

Since this transport is not necessarily parallel to the interior flow, it is likely to have a nonzero divergence. Indeed

$$\begin{aligned}\frac{\partial U_i}{\partial x} + \frac{\partial V_i}{\partial x} &= \int_0^\infty \left(\frac{\partial u}{\partial x} + \frac{\partial v}{\partial y}\right)dz \\ &= -\frac{d_B}{2}\left(\frac{\partial \overline{v}}{\partial x} - \frac{\partial \overline{u}}{\partial y}\right) \\ &= -\frac{d_B}{2\rho_0 f}\nabla^2 \bar{p'}_i i = 0, 1, 2, 3 \cdots,\end{aligned} \tag{17}$$

where $\overline{p}'_i = \overline{p}_i - \overline{p}_{i-1}$.

Then the vertical velocity in the interior can be evaluated by a vertical of the continuity equation, using $w(z = 0) = 0$ and $w(z = \pi d) = \overline{w}$:

$$\overline{w_i} = -\int_0^\infty \left(\frac{\partial u}{\partial x} + \frac{\partial v}{\partial y}\right)dz = \frac{d_B}{2}\left(\frac{\partial \overline{v}}{\partial x} - \frac{\partial \overline{u}}{\partial y}\right) = \frac{d_B}{2\rho_0 f}\nabla^2 \overline{p}'_i \tag{18}$$

Therefore, the vertical velocity W_i in the i layer is:

$$W_i = \sum_{i=i}^{i=n} \overline{w_i} = \frac{d_B}{2\rho_0 f}\nabla^2 \bar{p'}_i + \frac{d_B}{2\rho_0 f}\nabla^2 \overline{p}'_{i+1} + \cdots + \frac{d_B}{2\rho_0 f}\nabla^2 \overline{p}'_n i = 0, 1, 2, 3 \cdots \tag{19}$$

When $n \to \infty$, we can obtain the integration of W_0 in the surface as follows

$$W_0 = \int_{-\infty}^0 \overline{w_i}dz = \frac{d_B}{2\rho_0 f}\nabla^2 p_0 \tag{20}$$

In the cylinder coordinate system, the W_b in the entire water column is as follow(the process is provided in the Appendix 54):

$$W_b = \frac{d_B}{2\rho_0 f}\left(\frac{\partial^2 p}{\partial r^2} + \frac{1}{r}\frac{\partial p}{\partial r}\right). \tag{21}$$

On this basis, the motion state of the water in the ideal ocean and wind field can be calculated. Within the range of the maximum wind, downwelling in the surface is caused by the classical Ekman layer theory and upwelling is caused by the quasi-bottom Ekman. Specifically, ocean water converges in an inward spiral in the deeper layer and diverges in the upper layer to form a water elevation field with low center and high surroundings. In turn, the pressure gradient force that is proportional to water elevation drives the cyclogeostrophic current. Because of the circular motion, part of the pressure gradient force is provided to the centripetal force. Therefore, the pressure gradient force decreases with increasing depth, which leads to different currents in the upper and deeper layers. Then, because of the occurrence of friction, which is similar to the bottom Ekman pump leading to upwelling, when the pressure gradient force disappears, the ocean water stops its dynamic behavior and upwelling does not occur, showed in Fig. 1.

2.3 Depth impacted by typhoon

According to the aforementioned analysis, to estimate the impacted depth, we must obtain certain variables, including p, f, and r_0. Because their ranges are very large, a magnitude scale is used, wherein wind stress is $\tau = 5\ \mathrm{N/s^2}$, the maximum water elevation (from the maximum water elevation under the typhoon wind-current to the center of typhoon where the water elevation is the lowest) is $\xi = 0.5$ m, the Coriolis parameter is $f = 4.96 \times 10^{-5}$ rad/s (approximately 20 °N), $\pi d_T = 100$ m, $\pi d_B = 100$ m, $r_0 = 50$ km, $\rho_0 = 1.025 \times 10^3\ \mathrm{kg/m^3}$, and gravitational acceleration is $\mathrm{g} = 9.8\ \mathrm{kg \cdot m/s^2}$. According to this scale of the variables, the surface Ekman layer vertical velocity w_s(Eq. 4) and quasi-bottom Ekman layer vertical velocity w_b (Eq. 15) with $v_\theta = 1$ m/s are shown in Fig. 2.

Then, we can estimate the azimuthal velocity v_θ (Eq. 11) in a homogenous ocean, as shown in Fig. 3.

According to Fig. 3, v_θ in the surface layer is approximately1.3 m/s, and decreases with increasing depth. Then, when the depth reaches 1.0×10^4 m, v_θ is approximately 0.3 m/s. Below this depth, v_θ reduces very slowly, allowing

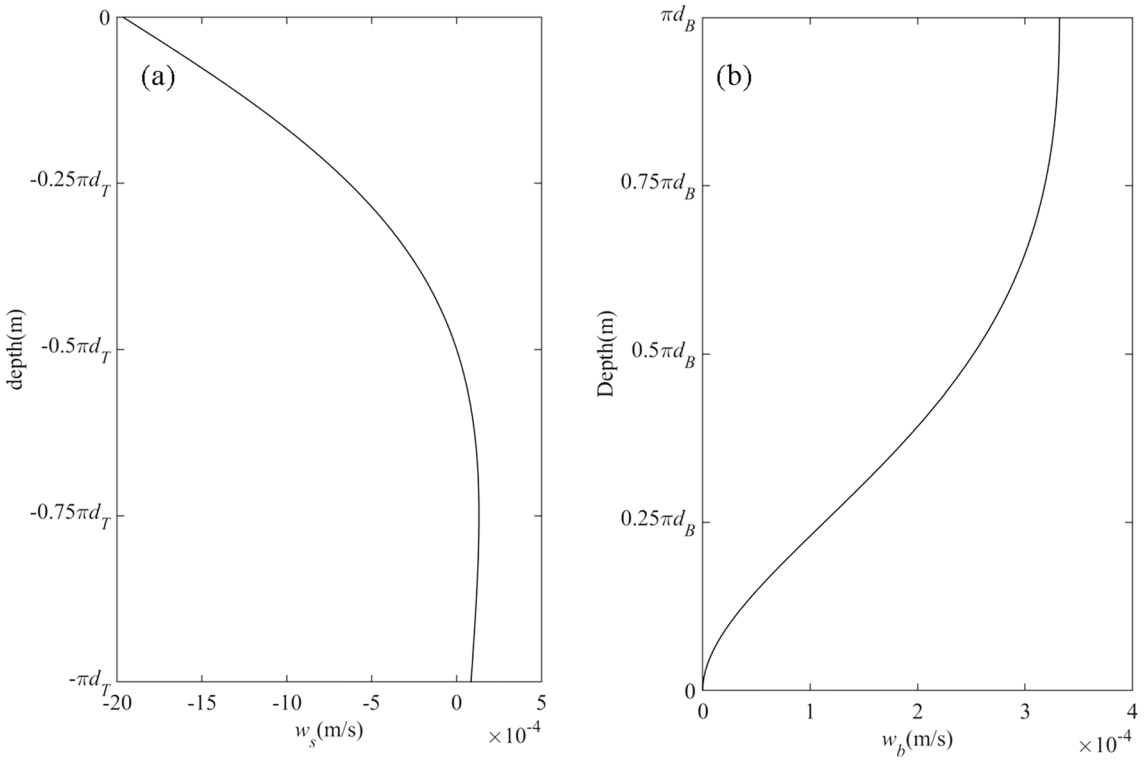

Fig. 2 Vertical velocities caused by Ekman transport. (**a**) w_s the vertical velocity caused by surface Ekman transport; (**b**) w_b the vertical velocity caused by the quasi-bottom Ekman transport

it to extend to very deep water, and is approximately 0.05 m/s at the depth of 5.0×10^4 m.

In an actual ocean, density is not a constant, making it very complex. For simplicity, we assumed that the entire water column is raised by $d\prime$=100 m in the center of the typhoon but stays the same in the radius r_0, maintaining a linear variation between them. Thus, we can calculate the barocline. The initial density was observed in the Pacific at 127.525 °E and 20.456 °N in April 2009 (Fig. 4).

We let the depth of water rise $d\prime$=100 m to represent the impact of the typhoon. On this basis, the horizontal momentum equation changes as follows:

$$\frac{1}{\rho}\frac{\partial p}{\partial r}=fv_\theta+\frac{v_\theta^2}{r_0}+\frac{1}{\rho}\frac{\partial p_{\text{barocline}}}{\partial r}, \tag{22}$$

where $p_{\text{barocline}}$ is the barocline caused by different densities.

The solution of v_θ is easy to obtain using this equation. Under this assumption, the vertical variation of v_θ is shown in Fig. 5.

In the real ocean, v_θ decreases faster than in the idealized ocean, becoming zero at a depth of approximately 2200 m. Therefore, according to our assumption, a typhoon can influence ocean water below 2200 m. Furthermore, if we neglect radial variation, which would make v_θ uniform, W_b can be calculated using Eq. (21), and the vertical velocity $w = w_s + W_b$ in the entire water column as shown in Fig. 6.

The results indicate that w decreases as it nears the surface. In particular, its maximum value is approximately 1.7×10^{-3} m/s at the depth of approximately 80 m, as determined by several parameters, including the quasi-bottom Ekman depth d_B, azimuthal velocity v_θ, and so on.

2.4 Sensitivity experiments

In fact, the intensity and size of typhoons are varied and p_0 will change with them, but the functional relation is very hard to get. For simplicity, we only consider ξ, $d\prime$, r_0, in-situ density and keep the other variables the formers. We can estimate the maximum depth $d_{\max}$ impacted by the typhoon by determining where the vertical velocity w

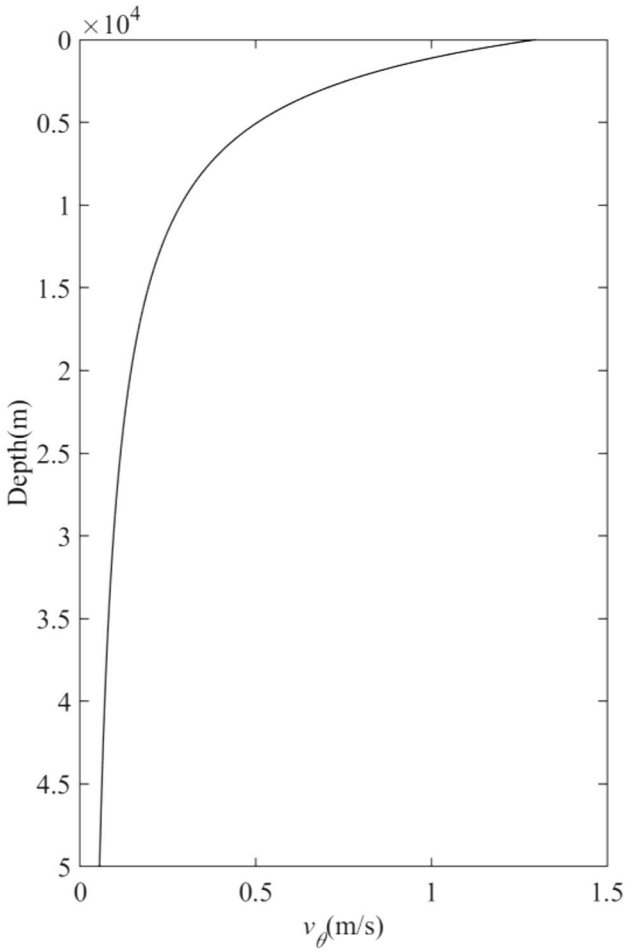

Fig. 3 Azimuthal velocity v_θ in a homogenous ocean

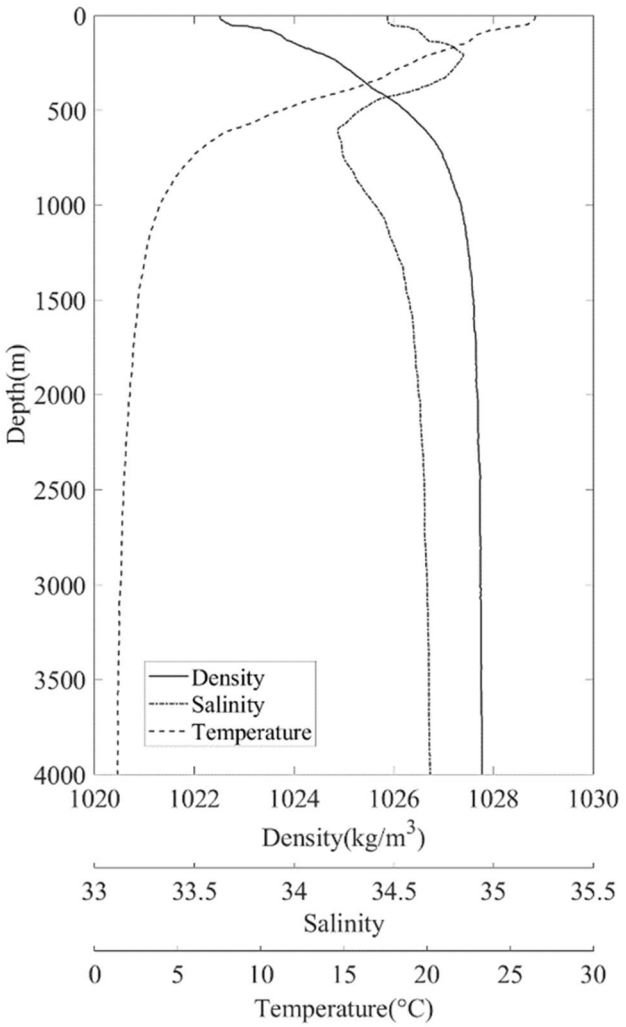

Fig. 4 In-situ Pacific observation data at 127.525 °E and 20.456 °N in April 2009

approaches zero. Note that the depth of observation data in Fig. 4 is 4000 m, so we can only estimate w within the depth. When $d_{\max}$ is deeper than 4000 m, it is equal to 4000 m.

If we let $\xi = 0.5$ m, $0 \le d\prime \le 200$ m, 10 km $\le r_0 \le$ 100 km and then $d_{\max}$ is shown in Fig. 7.

If we let $d\prime = 100$ m, $0 \le \xi \le 1$ m, 10 km $\le r_0 \le 100$ km and then $d_{\max}$ is shown in Fig. 8.

If we let $r_0 = 50$ km, $0 \le \xi \le 1$ m, $0 \le d\prime \le 200$ m, and then $d_{\max}$ is shown in Fig. 9.

These results when compared with the density distribution shown in Fig. 4 are interesting. Specifically, because of the small density variation, the maximum depth impacted by the typhoon is very sensitive to the water elevation below 1000 m, which is consistent with the results shown in Fig. 3, which displays a homogenous ocean. However, in reality, the water elevation and the depth of water rising are not ergodic, and thus the depth impacted by the typhoon could not reach the whole depth shown in Figs. 7, 8 and 9.

3 Results and discussion

According to the vertical velocity analysis of the entire water column, the pressure gradient force caused by surface Ekman transport impacts deep ocean water by providing centripetal force and balancing with the barocline. Different currents driven by different pressure gradient forces produce friction that is consistent with the quasi-bottom Ekman layer leading to upwelling. When the pressure gradient force disappears, the ocean water loses this

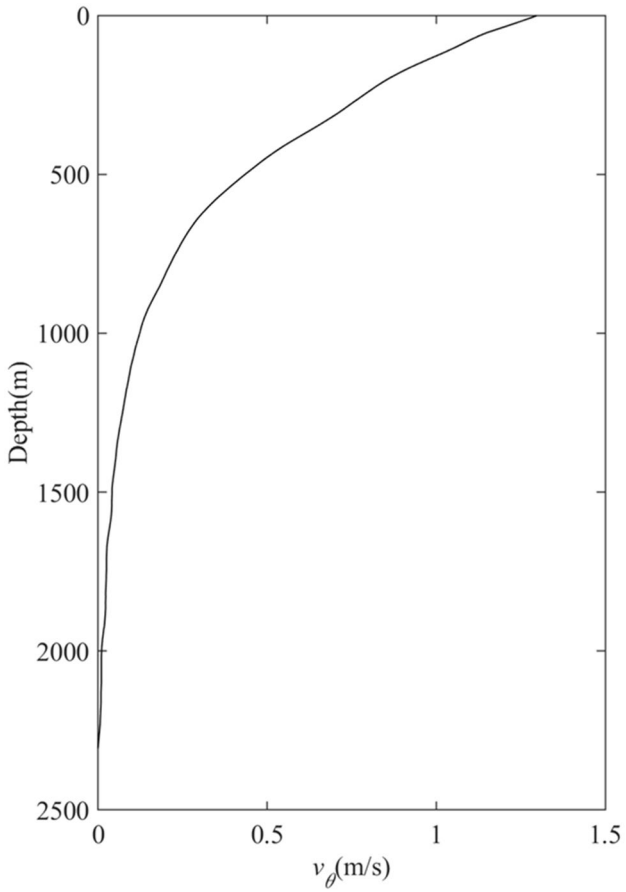

Fig. 5 Azimuthal velocity v_θ in the baroclinic ocean

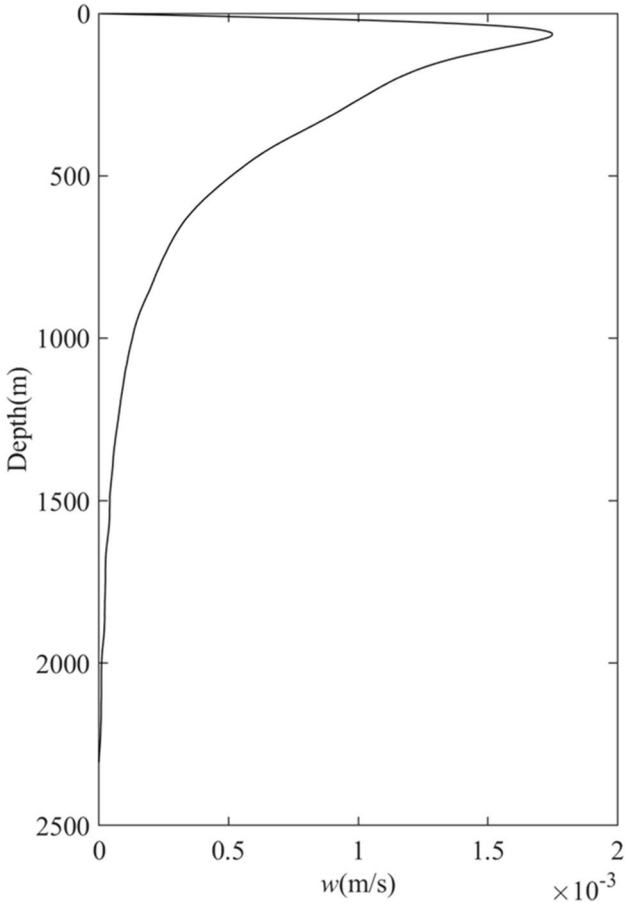

Fig. 6 Vertical velocity w caused by typhoon

dynamic relationship, and upwelling ceases. The depth impacted by a typhoon can reach greater than 1000 m and even more.

In this study, we only considered advection without any diffusion. There are two Ekman pumpings in ocean water, one in the surface layer caused by Ekman transport and the other exists in the entire water column which is caused by pressure gradient force (Fig. 10).

4 Conclusions

This study shows the analytical solutions on typhoon-induced upwelling under idealized typhoon and ocean conditions, and simply divides the ocean into two parts, the Ekman layer and the lower layer. The analytical solutions are derived from the pressure gradient force, centripetal force, Coriolis force, and baroclinic pressure-gradient force. Using the analytical solutions, we successfully calculate the maximum depth impacted by the idealized typhoon and ocean characterized by given parameters.

The pressure-gradient force, caused by typhoons and then offset by centripetal and baroclinic forces, is the original dynamic of upwelling in deep ocean water. While some of the assumptions in this study are substantial and the dynamic mechanism analysis of upwelling for a stationary typhoon is highly idealized, we evaluated several important variables, including water elevation, radius of maximum circular motion, depth of water column rising, and in-situ density. Because inertial pumping and entrainment play important roles in the vertical turbulent mixing process, to estimate the depth impacted by typhoons, we used special values that have a strong link with vertical velocity and impacted depth. Further, when possible, we obtained in-situ ocean observation data. It could be a part of study to explain the results.

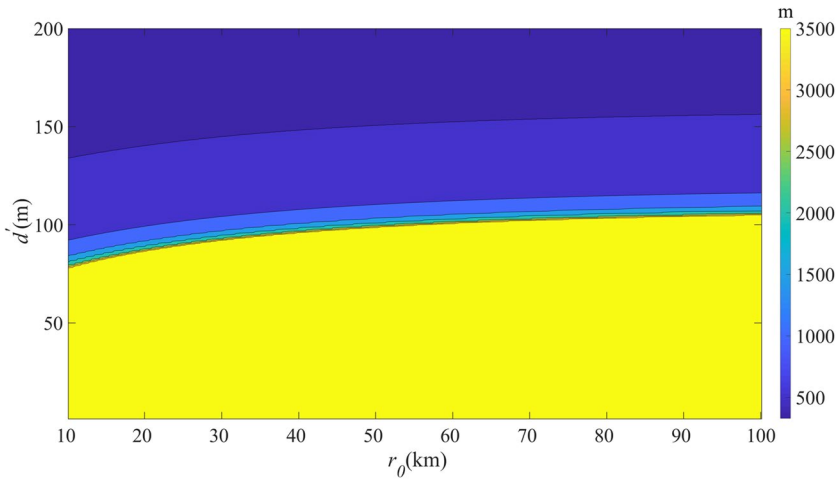

Fig. 7 The maximum depth d_{max} impacted by the typhoon (ξ= 0.5 m)

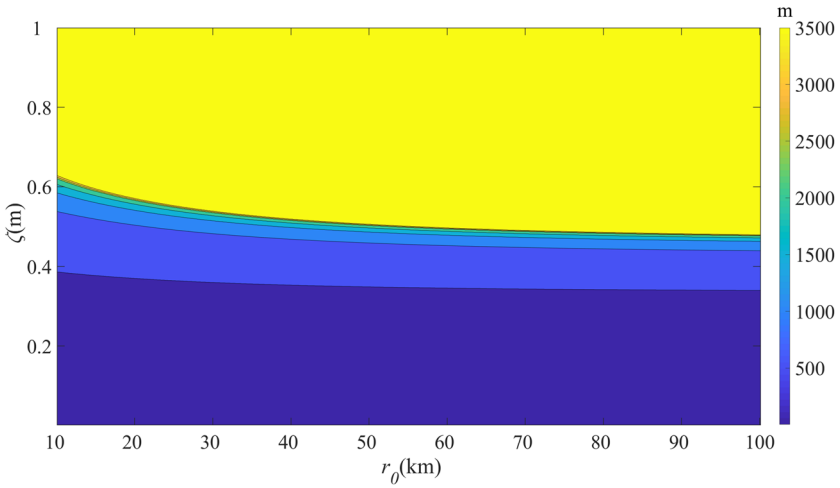

Fig. 8 The maximum depth d_{max} impacted by the typhoon (d'= 100 m)

A moving typhoon creates a very complex dynamic process. Thus, the circulation effects of a passing typhoon are of interest. Although the use of stationary Ekman theory in a homogenous ocean is far removed from the actual situation, this study provides a succinct description of deep ocean upwelling caused by a stationary typhoon. Nevertheless, more extensively detailed research on the dynamic mechanism of deep ocean water rising is ongoing.

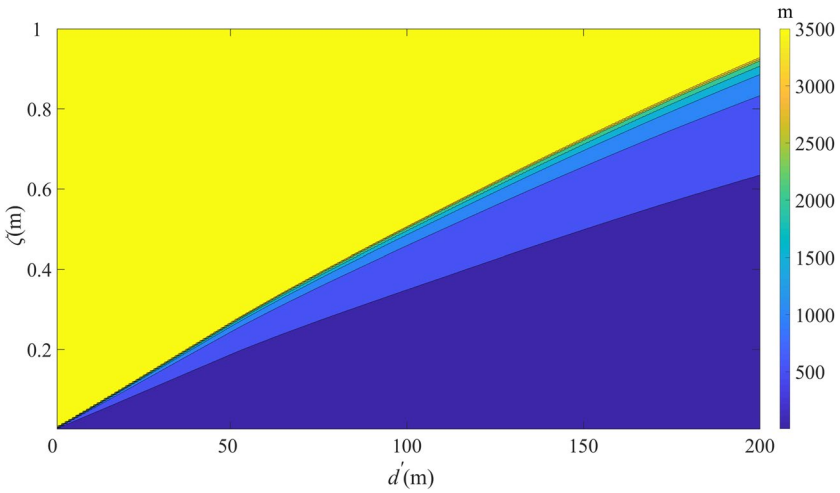

Fig. 9 The maximum depth d_{max} impacted by the typhoon (r_0= 50 km)

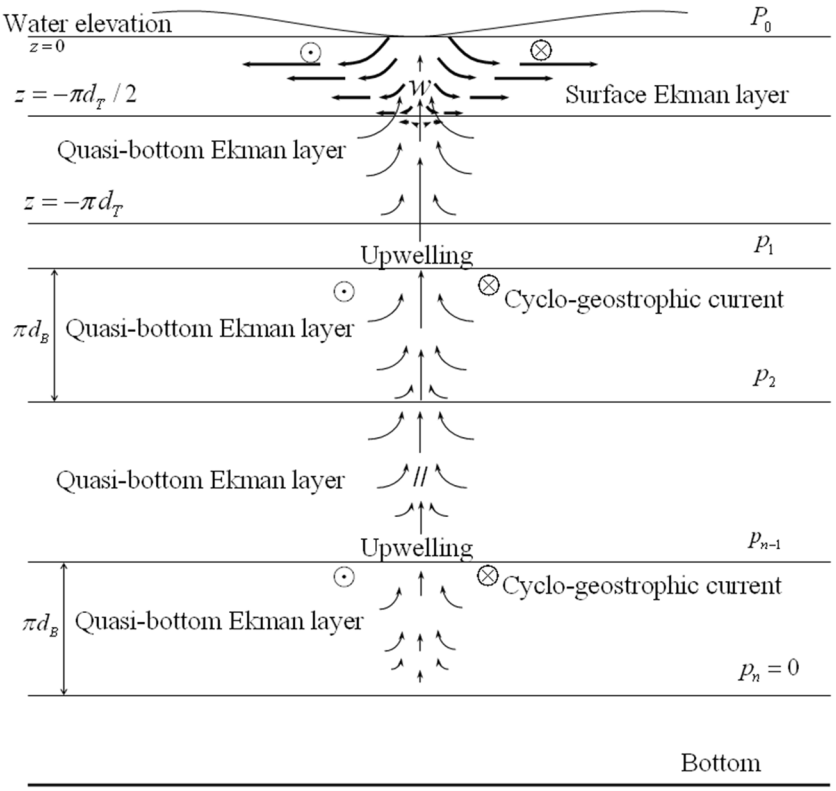

Fig. 10 Sketch of the upwelling caused by typhoon

5 Data availability

The observation data used in this manuscript have been archived by the College of Ocean and Earth Sciences, Xiamen University. The corresponding author can be contacted for information to access the archived data.

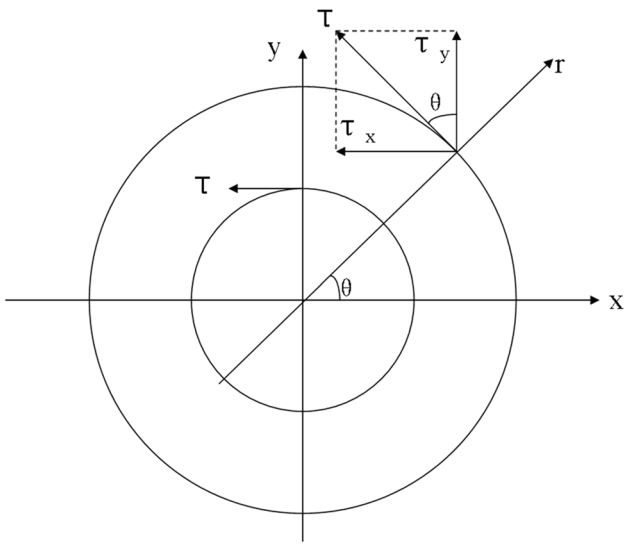

Fig. 11 The idealized wind-stress and coordinate system translation

Appendix

The wind-stress $\boldsymbol{\tau}$ is anticlockwise associated with the wind field of the typhoon and we assume that $\boldsymbol{\tau}$ is axis symmetry and divergence free, i.e. $\nabla \cdot \boldsymbol{\tau}=0$, as shown in Fig. 11.

The Cartesian coordinate system (x, y, z) can be translated into a cylinder coordinate system (r, θ, z).

$$\begin{cases} r = \sqrt{x^2 + y^2} \\ \theta = arctan\frac{y}{x} \\ z = z \end{cases} \tag{23}$$

The magnitude of $\boldsymbol{\tau}$ is τ and the direction is azimuthal, then:

$$\begin{cases} \tau_x = -\tau\ sin\theta \\ \tau_y = \tau\ cos\theta \end{cases}, \tag{24}$$

and

$$\begin{cases} x = r\ cos\theta \\ y = r\ sin\theta \end{cases}. \tag{25}$$

Therefore,

$$\frac{\partial r}{\partial x} = \frac{\partial\sqrt{x^2+y^2}}{\partial x} = \frac{x}{\sqrt{x^2+y^2}} = \frac{x}{r} = cos\theta \tag{26}$$

$$\frac{\partial r}{\partial y} = \frac{\partial\sqrt{x^2+y^2}}{\partial y} = \frac{y}{\sqrt{x^2+y^2}} = \frac{y}{r} = sin\theta, \tag{27}$$

$$\frac{\partial\theta}{\partial x} = \frac{\partial\left(arctan\frac{y}{x}\right)}{\partial x} = -\frac{sin\theta}{r}, \tag{28}$$

$$\frac{\partial\theta}{\partial y} = \frac{\partial\left(arctan\frac{y}{x}\right)}{\partial y} = \frac{cos\theta}{r}, \tag{29}$$

$$\frac{\partial\theta}{\partial r} = 0, \tag{30}$$

$$\frac{\partial\tau}{\partial\theta} = 0. \tag{31}$$

According to the derivation chain rule, we can obtain:

$$\frac{\partial\tau_y}{\partial x} = \frac{\partial\tau_y}{\partial r}\frac{\partial r}{\partial x} + \frac{\partial\tau_y}{\partial\theta}\frac{\partial\theta}{\partial x} = \frac{\partial\tau}{\partial r}cos^2\theta + \frac{\tau}{r}sin^2\theta, \tag{32}$$

$$-\frac{\partial\tau_x}{\partial y} = \frac{\partial\tau_x}{\partial r}\frac{\partial r}{\partial y} + \frac{\partial\tau_x}{\partial\theta}\frac{\partial\theta}{\partial y} = \frac{\partial\tau}{\partial r}sin^2\theta + \frac{\tau}{r}cos^2\theta, \tag{33}$$

$$\frac{\partial\tau_x}{\partial x} = \frac{\partial\tau_x}{\partial r}\frac{\partial r}{\partial x} + \frac{\partial\tau_x}{\partial\theta}\frac{\partial\theta}{\partial x} = -\frac{\partial\tau}{\partial r}cos\theta sin\theta + \frac{\tau}{r}sin\theta cos\theta \tag{34}$$

$$\frac{\partial\tau_y}{\partial y} = \frac{\partial\tau_y}{\partial r}\frac{\partial r}{\partial y} + \frac{\partial\tau_y}{\partial\theta}\frac{\partial\theta}{\partial y} = \frac{\partial\tau}{\partial r}sin\theta cos\theta - \frac{\tau}{r}cos\theta sin\theta. \tag{35}$$

Thus, the differential formulae of the surface vertical velocity is:

$$\begin{aligned}
\frac{\partial w_s}{\partial z} &= -\left(\frac{\partial u}{\partial x} + \frac{\partial v}{\partial y}\right)\\
&= -\frac{\sqrt{2}}{\rho_0 fd}e^{\frac{z}{d}}\left[\frac{\partial\tau_x}{\partial x}\sin\left(\frac{\pi}{4}+\frac{z}{d}\right) + \frac{\partial\tau_y}{\partial x}\cos\left(\frac{\pi}{4}+\frac{z}{d}\right) - \frac{\partial\tau_x}{\partial y}\cos\left(\frac{\pi}{4}+\frac{z}{d}\right) + \frac{\partial\tau_y}{\partial y}\sin\left(\frac{\pi}{4}+\frac{z}{d}\right)\right]\\
&= -\frac{\sqrt{2}}{\rho_0 fd}e^{\frac{z}{d}}\left[\left(\frac{\partial\tau_y}{\partial x} - \frac{\partial\tau_x}{\partial y}\right)\cos\left(\frac{\pi}{4}+\frac{z}{d}\right) + \left(\frac{\partial\tau_x}{\partial x} + \frac{\partial\tau_y}{\partial y}\right)\sin\left(\frac{\pi}{4}+\frac{z}{d}\right)\right]\\
&= -\frac{\sqrt{2}}{\rho_0 fd}e^{\frac{z}{d}}\left[\begin{array}{c}\left(\frac{\partial\tau}{\partial r}\cos^2\theta + \frac{\tau}{r}\sin^2\theta + \frac{\partial\tau}{\partial r}\sin^2\theta + \frac{\tau}{r}\cos^2\theta\right)\cos\left(\frac{\pi}{4}+\frac{z}{d}\right) +\\ \left(-\frac{\partial\tau}{\partial r}\cos\theta\sin\theta + \frac{\tau}{r}\sin\theta\cos\theta + \frac{\partial\tau}{\partial r}\sin\theta\cos\theta - \frac{\tau}{r}\cos\theta\sin\theta\right)\sin\left(\frac{\pi}{4}+\frac{z}{d}\right)\end{array}\right].\\
&= -\frac{\sqrt{2}}{\rho_0 fd}e^{\frac{z}{d}}\left(\frac{\partial\tau}{\partial r} + \frac{\tau}{r}\right)cos\left(\frac{\pi}{4}+\frac{z}{d}\right)
\end{aligned} \tag{36}$$

If it is similar to the surface, we can obtain the differential formulae of the bottom Ekman layer using the following:

$$\begin{aligned}
c\frac{\partial w_b}{\partial z} &= -\left(\frac{\partial u}{\partial x} + \frac{\partial v}{\partial y}\right) = -\frac{\partial\overline{u}}{\partial x}\left(1 - e^{-\frac{z}{d}}cos\frac{z}{d}\right)\\
&\quad + \frac{\partial\overline{v}}{\partial x}e^{-\frac{z}{d}}sin\frac{z}{d} - \frac{\partial\overline{v}}{\partial y}\left(1 - e^{-\frac{z}{d}}cos\frac{z}{d}\right) - \frac{\partial\overline{u}}{\partial y}e^{-\frac{z}{d}}sin\frac{z}{d}.\\
&= e^{-\frac{z}{d}}\left(\frac{\partial v_\theta}{\partial r} + \frac{v_\theta}{r}\right)sin\frac{z}{d}
\end{aligned} \tag{37}$$

The solution of Eq. (14) can be calculated as follows:

$$\begin{aligned}
w_s &= \int\frac{\partial w_s}{\partial z}dz\\
&= -\frac{\sqrt{2}}{\rho_0 fd}\left(\frac{\partial\tau}{\partial r} + \frac{\tau}{r}\right)\int e^{\frac{z}{d}}\cos\left(\frac{\pi}{4}+\frac{z}{d}\right)dz\\
&= -\frac{\sqrt{2}}{\rho_0 fd}\left(\frac{\partial\tau}{\partial r} + \frac{\tau}{r}\right)\left(e^{-\frac{\pi}{r}}d\int e^{\frac{z}{d}+\frac{\pi}{4}}\cos\left(\frac{z}{d}+\frac{\pi}{4}\right)d\left(\frac{z}{d}+\frac{\pi}{4}\right)\right)\\
&= -\frac{\sqrt{2}}{\rho_0 fd}\left(\frac{\partial\tau}{\partial r} + \frac{\tau}{r}\right)e^{-\frac{\pi}{r}}d\left(\frac{1}{2}e^{\frac{z}{d}+\frac{\pi}{r}}\left(\sin\left(\frac{z}{d}+\frac{\pi}{r}\right) + \cos\left(\frac{z}{d}+\frac{\pi}{4}\right)\right) + C_0\right)\\
&= -\frac{1}{\rho_0 f}e^{\frac{z}{d}}\left(\frac{\partial\tau}{\partial r} + \frac{\tau}{r}\right)\cos\frac{z}{d} + C_1
\end{aligned} \tag{38}$$

The solution of Eq. (15) can be calculated as follows:

$$\begin{aligned}
w_b &= \int\frac{\partial w_b}{\partial z}dz\\
&= \int\left(\frac{\partial v_\theta}{\partial r} + \frac{v_\theta}{r}\right)de^{-\frac{z}{d}}sin\left(-\frac{z}{d}\right)d\left(-\frac{z}{d}\right)\\
&= \left(\frac{\partial v_\theta}{\partial r} + \frac{v_\theta}{r}\right)\left(\frac{d}{2}e^{-\frac{z}{d}}\left(sin\left(-\frac{z}{d}\right) - cos\left(-\frac{z}{d}\right)\right) + C\right)\\
&= \left(\frac{\partial v_\theta}{\partial r} + \frac{v_\theta}{r}\right)\left(-\frac{\sqrt{2}d}{2}e^{-\frac{z}{d}}sin\left(\frac{z}{d}+\frac{\pi}{4}\right) + C\right)
\end{aligned} \tag{39}$$

In the cylinder coordinate system, the W in the entire water column is obtained as follow:

$$\frac{\partial p}{\partial x} = \frac{\partial p}{\partial r}\frac{\partial r}{\partial x} + \frac{\partial p}{\partial\theta}\frac{\partial\theta}{\partial x} \tag{40}$$

$$\frac{\partial p}{\partial y} = \frac{\partial p}{\partial r}\frac{\partial r}{\partial y} + \frac{\partial p}{\partial\theta}\frac{\partial\theta}{\partial y} \tag{41}$$

Using Eqs. (4)-(7), the equations are now

$$\frac{\partial p}{\partial x} = cos\theta\frac{\partial p}{\partial r} - \frac{sin\theta}{r}\frac{\partial p}{\partial\theta} \tag{42}$$

$$\frac{\partial p}{\partial y} = sin\theta \frac{\partial p}{\partial r} + \frac{cos\theta}{r} \frac{\partial p}{\partial \theta}. \tag{43}$$

Then, we obtain

$$\begin{aligned} \frac{\partial^2 p}{\partial x^2} =& \frac{\partial}{\partial x}\left(\frac{\partial p}{\partial x}\right) = cos\theta \frac{\partial}{\partial r}\left(\frac{\partial p}{\partial r} cos\theta - \frac{sin\theta}{r}\frac{\partial p}{\partial \theta}\right) \\ & - \frac{sin\theta}{r}\frac{\partial}{\partial \theta}\left(\frac{\partial p}{\partial r} cos\theta - \frac{sin\theta}{r}\frac{\partial p}{\partial \theta}\right) \end{aligned} \tag{44}$$

$$\begin{aligned} \frac{\partial^2 p}{\partial y^2} =& \frac{\partial}{\partial y}\left(\frac{\partial p}{\partial y}\right) = sin\theta \frac{\partial}{\partial r}\left(sin\theta \frac{\partial p}{\partial r} + \frac{cos\theta}{r}\frac{\partial p}{\partial \theta}\right) \\ & + \frac{cos\theta}{r}\frac{\partial}{\partial \theta}\left(sin\theta \frac{\partial p}{\partial r} + \frac{cos\theta}{r}\frac{\partial p}{\partial \theta}\right) \end{aligned} \tag{45}$$

The four terms on the right side of the equations (B-14) and (B-15) are as follows:

$$\begin{aligned} & cos\theta \frac{\partial}{\partial r}\left(\frac{\partial p}{\partial r} cos\theta - \frac{sin\theta}{r}\frac{\partial p}{\partial \theta}\right) \\ & = cos^2\theta \frac{\partial^2 p}{\partial r^2} + \frac{sin\theta cos\theta}{r^2}\frac{\partial p}{\partial \theta} - \frac{sin\theta cos\theta}{r}\frac{\partial^2 p}{\partial r \partial \theta} \end{aligned} \tag{46}$$

$$\begin{aligned} -\frac{sin\theta}{r}\frac{\partial}{\partial \theta}\left(\frac{\partial p}{\partial r} cos\theta - \frac{sin\theta}{r}\frac{\partial p}{\partial \theta}\right) =& -\frac{sin\theta cos\theta}{r}\frac{\partial^2 p}{\partial r \partial \theta} \\ & + \frac{sin^2\theta}{r}\frac{\partial p}{\partial r} + \frac{sin\theta cos\theta}{r^2}\frac{\partial p}{\partial \theta} + \frac{sin^2\theta}{r^2}\frac{\partial^2 p}{\partial \theta^2} \end{aligned} \tag{47}$$

$$\begin{aligned} sin\theta \frac{\partial}{\partial r}\left(sin\theta \frac{\partial p}{\partial r} + \frac{cos\theta}{r}\frac{\partial p}{\partial \theta}\right) =& sin^2\theta \frac{\partial^2 p}{\partial r^2} \\ & - \frac{sin\theta cos\theta}{r^2}\frac{\partial p}{\partial \theta} + \frac{sin\theta cos\theta}{r}\frac{\partial^2 p}{\partial r \partial \theta} \end{aligned} \tag{48}$$

$$\begin{aligned} \frac{cos\theta}{r}\frac{\partial}{\partial \theta}\left(sin\theta \frac{\partial p}{\partial r} + \frac{cos\theta}{r}\frac{\partial p}{\partial \theta}\right) =& \frac{cos^2\theta}{r}\frac{\partial p}{\partial r} \\ & + \frac{sin\theta cos\theta}{r}\frac{\partial^2 p}{\partial \theta \partial r} - \frac{sin\theta cos\theta}{r^2}\frac{\partial p}{\partial \theta} + \frac{cos^2\theta}{r^2}\frac{\partial^2 p}{\partial \theta^2}. \end{aligned} \tag{49}$$

Therefore, we get

$$\nabla^2 p = \frac{\partial^2 p}{\partial r^2} + \frac{1}{r}\frac{\partial p}{\partial r} + \frac{1}{r^2}\frac{\partial^2 p}{\partial \theta^2} \tag{50}$$

Along an isobar, the pressure is const, Thus

$$\frac{\partial p}{\partial \theta} = 0 \tag{51}$$

and

$$\frac{\partial^2 p}{\partial \theta^2} = 0. \tag{52}$$

Then, we obtain the Laplace operator of p in the cylinder coordinate system:

$$\nabla^2 p = \frac{\partial^2 p}{\partial r^2} + \frac{1}{r}\frac{\partial p}{\partial r}. \tag{53}$$

So, we get the vertical velocity caused by bottom Ekman at the role of p as follow:

$$W = \frac{d_B}{2\rho_0 f}\left(\frac{\partial^2 p}{\partial r^2} + \frac{1}{r}\frac{\partial p}{\partial r}\right). \tag{54}$$

Acknowledgements I thank Professor Jianyu Hu for providing the observation data and Professor Yuwu Jiang for helping to guide this research. This work was supported by the Marine Economic Development Subsidy Project of Fujian, China [grant number ZHHY-2019-2]; the National Natural Science Foundation of China [grant number 91958203]; and the National Key R&D Program of China [grant number 2017YFC1404804].

Declarations The authors declare that they have no known competing financial interests or personal relationships that could have appeared to influence the work reported in this paper.

References

Babin SM, Carton JA, Dickey TD, Wiggert JD (2004) Satellite evidence of hurricane-induced phytoplankton blooms in an oceanic desert. J Geophys Res 109(3):C03043. https://doi.org/10.1029/2003JC001938

Benoit CR, Beckers JM (2009) *Introduction to geophysical fluid dynamics physical and numerical aspects*. Academic Press, pp 828

Chang SW (1985) Deep ocean response to hurricanes as revealed by an ocean model with free surface. Part I: Axisymmetric case. J Phys Oceanogr 15(12):1847–1858. https://doi.org/10.1175/1520-0485(1985)0152.0.CO;2

Emanuel K (2003) Tropical cyclones. Annu Rev Earth Planet ScI 31:75–104. https://doi.org/10.1146/annurev.earth.31.100901.141259

Gierach MM, Subrahmanyam B (2008) Biophysical responses of the upper ocean to major Gulf of Mexico hurricanes in 2005. J Geophys Res Oceans 113(C4):C04029. https://doi.org/10.1029/2007JC004419

Ginis I, Sutyrin G (1995) Hurricane-generated depth-averaged currents and sea surface elevation. J Phys Oceanogr 25:1218–1242. https://doi.org/10.1175/1520-0485(1995)025%3c1218:HGDACA%3e2.0.CO;2

Hopkins CK (1982) Ocean response to hurricane forcing. M. S. thesis, Dept. of Science in Meteorology and Oceanography, Naval Postgraduate School, pp 89

Jansen M, Ferrari R (2009) Impact of the latitudinal distribution of tropical cyclones on ocean heat transport. Geophys Res Lett 36:L06604. https://doi.org/10.1029/2008GL036796

Leipper DF (1967) Observed ocean conditions and hurricane Hilda, 1964. J Atmos Sci 24:182–196. https://doi.org/10.1175/1520-0469(1967)024%3c0182:OOCAHH%3e2.0.CO;2

Lin LL, Liu WT, Wu CC, Chiang JCH, Sui CH (2003) Satellite observations of modulation of surface winds by typhoon-induced

upper ocean cooling. Geophys Res Lett 30:1131–1134. https://doi.org/10.1029/2002GL015674
Liu ZH, Xu JP, Zhu BK, Sun CH, Zhang LF (2007) The upper ocean response to tropical cyclones in the northwestern Pacific analyzed with Argo data. Chin J Oceanol Limn 25:123–131. https://doi.org/10.1007/s00343-007-0123-8
Lu MZ, Huang RX (2010) The three-dimensional steady circulation in a Homogenous ocean induced by a stationary hurricane. J Phys Oceanogr 40(7):1441–1457. https://doi.org/10.1175/2010JPO4293.1
Morozov EG, Velarde MG (2008) Inertial oscillations as deep ocean response to hurricanes. J Oceanogr 64:495–509. https://doi.org/10.1007/s10872-008-0042-0
Price JF (1981) Upper ocean response to a hurricane. J Phys Oceanogr 11:153–175. https://doi.org/10.1175/1520-0485(1981)0112.0.CO;2
Price JF (1983) Internal wave wake of a moving storm. Part I: Scales, energy budget and observations. J Phys Oceanogr 13(6):949–965. https://doi.org/10.1175/1520-0485(1983)0132.0.CO;2
Price JF, Sanford TB, Forristall GZ (1994) Forced stage response to a moving hurricane. J Phys Oceanogr 24(2):233–260. https://doi.org/10.1175/1520-0485(1994)0242.0.CO;2
Pudov VD (1978) Vertical structure of the wake of a typhoon in the upper ocean. Okeanologiya 18:142–146
Shay LK, Elsberry RL (1987) Near-inertial ocean current response to Hurricane Frederic. J Phys Oceanogr 17(8):1249–1269. https://doi.org/10.1175/1520-0485(1987)017%3c1249:NIOCRT%3e2.0.CO;2
Spencer LJ, DiMarco SF, Wang ZK, Kuehl JJ, Brooks DA (2016) Asymmetric oceanic response to a hurricane: Deep water observations during Hurricane Isaac. J Geophys Res Oceans 121:7619–7649. https://doi.org/10.1002/2015JC011560
Taitra K, Kjtagawa S, Otobe H, Asai T (1993) Observation of temperature and velocity from a surface buoy moored in the Shikoku Basin (OMLET-88). J Oceanogr 49:397–406. https://doi.org/10.1007/BF02234956
Wada A (2005) Numerical simulations of sea surface cooling by a mixed layer model during the passage of typhoon Rex. J Oceanogr 61(1):41–57. https://doi.org/10.1007/s10872-005-0018-2
Wada A, Nino H, Nakano H (2009) Roles of vertical turbulent mixing in the ocean response to typhoon Rex (1998). J Oceanogr 65:373–396. https://doi.org/10.1007/s10872-009-0034-8
Zhang H, Chen DK, Zhou L, Liu XH, Ding T, Zhou BF (2016) Upper ocean response to typhoon Kalmaegi. J Geophys Res Oceans 121(8):6520–6535. https://doi.org/10.1002/2016JC012064
Zheng QA, Lai R, Huang NE, Pan JY, Liu WT (2006) Observation of ocean current response to 1998 Hurricane Georges in the Gulf of Mexico. Acta Oceanol Sin 25:1–14